This is the accepted manuscript made available via CHORUS. The article has been published as:

Double Dirac Semimetals in Three Dimensions

Benjamin J. Wieder, Youngkuk Kim, A. M. Rappe, and C. L. Kane

Phys. Rev. Lett. **116**, 186402 — Published 5 May 2016

DOI: 10.1103/PhysRevLett.116.186402

Double Dirac Semimetals in Three Dimensions

Benjamin J. Wieder,[1] Youngkuk Kim,[2] A. M. Rappe,[2] and C. L. Kane[1]
[1] *Department of Physics and Astronomy, University of Pennsylvania, Philadelphia, PA 19104-6323, USA*
[2] *The Makineni Theoretical Laboratories, Department of Chemistry, University of Pennsylvania, Philadelphia, PA 19104-6323, USA*

We study a class of Dirac semimetals that feature an eightfold-degenerate double Dirac point. We show that 7 of the 230 space groups can host such Dirac points and argue that they all generically display linear dispersion. We introduce an explicit tight-binding model for space groups 130 and 135. Space group 135 can host an intrinsic double Dirac semimetal with no additional states at the Fermi energy. This defines a symmetry-protected topological critical point, and we show that uniaxial compressive strain applied in different directions leads to topologically distinct insulating phases. In addition, the double Dirac semimetal can accommodate topological line defects that bind helical modes. Connections are made to theories of strongly interacting filling-enforced semimetals, and potential materials realizations are discussed.

A striking consequence of symmetry and topology in the electronic structure of materials is the existence of protected degeneracies that guarantee semimetallic behavior. Such degeneracies occur in graphene [1] (in the absence of spin-orbit interactions) as well as at the surface of a topological insulator (TI) [2]. In 2011, Wan et al. [3] pointed out that twofold degenerate Weyl points could occur in bulk 3 dimensional (3D) materials. Such Weyl points are topologically protected, though they are "symmetry prevented" in that they require broken inversion or time-reversal (T) symmetry to exist. Crystal symmetries can lead to a richer variety of nodal semimetals. Dirac semimetals [4–6], which feature fourfold degenerate Dirac points protected by crystal symmetry, occur in two varieties. Topological Dirac semimetals, such as Cd_3As_2 and Na_3Bi [7–9], exhibit Dirac points on a rotational symmetry axis due to a band inversion. Nonsymmorphic Dirac semimetals, predicted in BiO_2 [4] and in $BiZnSiO_4$ [10], conversely have Dirac points at high-symmetry points which are guaranteed by the underlying Space Group (SG) symmetry. Additional classes of nodal semimetals include line nodes [11–20] in 3D and Dirac semimetals in 2D [21, 22].

In this paper we introduce and analyze a double Dirac semimetal (DDSM) that exhibits a single eightfold degeneracy point at a Brillouin Zone (BZ) corner. We show that 7 of the 230 SGs host double Dirac points (DDPs) and argue that all of them generically have linear dispersion. For two of the SGs (130 and 135) a DDP is guaranteed whenever the band filling is an odd multiple of four, while for the remaining five SGs the presence of DDPs depends on the band ordering. We introduce an explicit tight-binding model for SGs 130 and 135 that demonstrates the DDP, and we study its low energy structure in detail. The DDSM has similar mobility and screening properties as the topological Dirac semimetal. However, the two differ fundamentally because the DDSM is symmetry tuned to a topological quantum critical point. Like the single (nonsymmorphic) Dirac semimetal, the DDSM can be gapped into a trivial or topological insulator by applying strain. In DDSMs, both phases can be achieved with compressive strain oriented along two different directions. Moreover, in the DDSM, spatially modulating the symmetry-breaking energy gap can lead to topological line defects that bind 1D helical modes. These features open new possibilities for topological band structure engineering. Materials hosting DDPs are discussed at the end of the paper.

Space Group			$\mathbf{K}$	Reps at $\mathbf{K}$	Vector Reps
130	$P4/ncc$	$\Gamma_q D_{4h}^8$	A	$\Gamma_5^{\oplus 2}(8)$	$4E_u \oplus 3A_{2u}$
135	$P4_2/mbc$	$\Gamma_q D_{4h}^{13}$	A	$\Gamma_5^{\oplus 2}(8)$	$4E_u \oplus 3A_{2u}$
218	$P\bar{4}3m$	$\Gamma_c T_d^4$	R	$\Gamma_6 \oplus \Gamma_7(4)$, $\Gamma_8^{\oplus 2}(8)$	$2T_2$
220	$P\bar{4}3d$	$\Gamma_c^v T_d^6$	H	$\Gamma_6 \oplus \Gamma_7(4)$, $\Gamma_8^{\oplus 2}(8)$	$2T_2$
222	$Pn3n$	$\Gamma_c O_h^2$	R	$\Gamma_5(4)$, $\Gamma_6 \oplus \Gamma_7(8)$	$3T_{1u}$
223	$Pm3n$	$\Gamma_c O_h^3$	R	$\Gamma_5(4)$, $\Gamma_6 \oplus \Gamma_7(8)$	$3T_{1u}$
230	$Ia3d$	$\Gamma_c^v O_h^{10}$	H	$\Gamma_5(4)$, $\Gamma_6 \oplus \Gamma_7(8)$	$3T_{1u}$

TABLE I. Space groups that host DDPs. SGs are indicated in International notation as well as in Shönflies notation, which indicates the crystal system and point group. The momenta $\mathbf{K}$ are listed with symmetry labels for the 8DIRs, as well as for some 4DIRs. The final column indicates the T-invariant vector representations of the point group contained in the tensor product $\Gamma^* \otimes \Gamma$ of the 8DIR at $\mathbf{K}$, indicating that in each case a linear dispersion is generic.

The existence of symmetry-protected degeneracies at a point $\mathbf{K}$ in the BZ can be ascertained by determining the dimension of the appropriate double-valued projective representations of the little group of $\mathbf{K}$. This information has been tabulated for all 230 SGs [23]. Table I lists all of the SGs with symmetry points that host Four-Dimensional Irreducible Representations (4DIR) that are also doubled by T symmetry[24].

SGs 130 and 135 have the distinguishing feature that there is only a single 8DIR at the A point. Therefore groups of 8 bands "stick together", implying an insulator is only possible when the band filling is a multiple of 8. Interestingly, Watanabe et al. [25](WPVZ) recently introduced a bound on the minimal filling for an insulator that applies to strongly-interacting systems. The WPVZ bound for SG 130 is 8, in agreement with the band theory analysis, while for SG 135 the WPVZ bound of 4 disagrees with band theory [25]. Below we show that for SG 130, but not for SG 135, additional single Dirac points are present when the filling is an odd multiple of 4. Since the energy of the single and DDPs will differ, SG 130 will generically host a semimetal with electron and hole pockets. In contrast, in SG 135 the DDP is the only required degeneracy, so SG 135 can host an intrinsic DDSM. The fact that the symmetry-guaranteed DDP is not covered by the WPVZ bound poses the interesting question of whether strong interactions can open a symmetry-preserving gap in SG 135.

For the remaining 5 SGs in Table I there are 4DIRs in addition to the 8DIRs at $\mathbf{K}$. Therefore, the presence of DDPs at the Fermi level depends on the band ordering, as it does in group IV semiconductors where band inversion in grey tin leads to a fourfold degeneracy at E_F [26] with quadratic dispersion. To determine whether the dispersion at the DDPs is linear we check whether the T-odd vector representation(s) are contained in the tensor product $\Gamma \otimes \Gamma^*$ of the 8DIR at $\mathbf{K}$ [4]. This is found by computing the character of the symmetric Kronecker square [23] of Γ and using the orthogonality of characters to project onto the vector representation. This analysis, which agrees with the specific example worked out below, predicts the multiple vector representations listed in Table I. Therefore in all cases the dispersion near $\mathbf{K}$ will generically be linear. The DDP is anisotropic for the tetragonal structures 130 and 135, while for the remaining cubic structures it is isotropic.

We now introduce an explicit tight-binding model for SGs 130 and 135. These SGs share the same tetragonal structure and are characterized by the symmetry generators in Table II. We introduce a unit cell (Fig. 1(a)), with 4 sublattices indexed by $(\tau^z, \mu^z) = (\pm 1, \pm 1)$ associated with basis vectors $\mathbf{d} = \frac{1}{2}[(1-\tau^z)(\frac{1}{2}\frac{1}{2}0) + (1-\mu^z)(00\frac{1}{2})]$. This can be viewed as a distortion of a parent Bravais lattice [21] in which the 4 sublattices are related by pure translations. Nearest neighbor hopping on this parent lattice is described by

$$\mathcal{H}_0(\mathbf{k}) = t_{xy}\tau^x \cos\tfrac{k_x}{2}\cos\tfrac{k_y}{2} + t_z\mu^x\cos\tfrac{k_z}{2}, \qquad (1)$$

where we choose a gauge in which the state associated with sublattice (τ^z, μ^z) has phase $\exp i\mathbf{k}\cdot\mathbf{d}$, so

$$\mathcal{H}(\mathbf{k}+\mathbf{G}) = e^{-i\mathbf{G}\cdot\mathbf{d}(\tau^z,\mu^z)}\mathcal{H}(\mathbf{k})e^{i\mathbf{G}\cdot\mathbf{d}(\tau^z,\mu^z)}. \qquad (2)$$

SGs 130 and 135 involve lowering the translational symmetry while keeping different nonsymmorphic glide and screw symmetries. The symmetry generators are represented by operators on the 8-dimensional spin and sublattice space $D(\{g|\mathbf{t}\})$ listed in Table II. In addition, T symmetry is represented by $\Theta = i\sigma^y K$. Symmetry-lowering perturbations $\mathcal{H} = \mathcal{H}_0 + V$ must satisfy

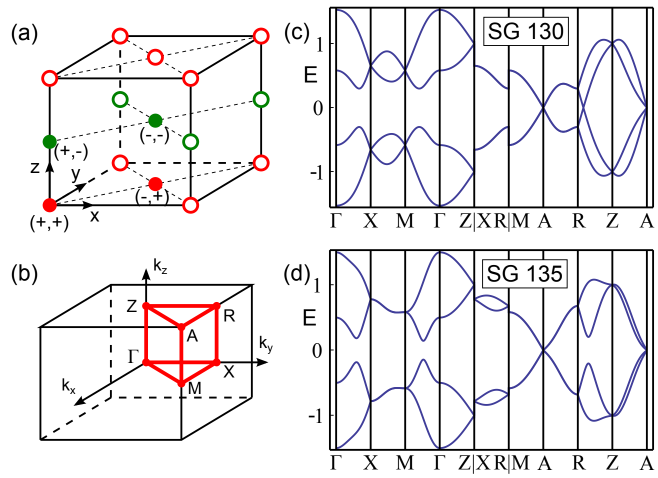

FIG. 1. (a) Model lattice for the common tetragonal structure of SGs 130 and 135. The solid lines indicate the four-site unit cell, and solid circles denote the 4 sublattices labeled by $(\tau^z, \mu^z) = (\pm, \pm)$. (b) Tetragonal Brillouin zone. (c) Energy bands for SG 130, described by the tight-binding model (1,5) with $t_{xy} = 1$, $t_z = 0.5$ and $\lambda_1 = \lambda_2 = \lambda_3 = 0.3$. In addition to the DDP at A, there is a symmetry-guaranteed Dirac point on the line Z-R. (b) Bands for SG 135, described by (1,6) with $t_{xy} = 1$, $t_z = 0.5$, $t_1' = t_2' = 0.3$, $\lambda_1' = 0.3$, $\lambda_2' = 0.1$, $\lambda_3' = 0.25$. There is a single DDP at A with no other crossings.

SG 130		SG 135	
$\{g\|\mathbf{t}\}$	$D(\{g\|\mathbf{t}\})$	$\{g\|\mathbf{t}\}$	$D(\{g\|\mathbf{t}\})$
$\{C_{4z}\|000\}$	$e^{i\pi\sigma^z/4}$	$\{C_{4z}\|00\frac{1}{2}\}$	$\mu^x e^{i\pi\sigma^z/4}$
$\{C_{2x}\|\frac{1}{2}\frac{1}{2}0\}$	$i\tau^x\sigma^x$	$\{C_{2x}\|\frac{1}{2}\frac{1}{2}0\}$	$i\tau^x\sigma^x$
$\{I\|\frac{1}{2}\frac{1}{2}\frac{1}{2}\}$	$\tau^x\mu^x$	$\{I\|000\}$	1

TABLE II. Symmetry generators for SGs 130 and 135, along with their representations in the sublattice-spin space.

$$V(g\mathbf{k}) = D(\{g|\mathbf{t}\})^\dagger V(\mathbf{k}) D(\{g|\mathbf{t}\}), \qquad (3)$$
$$V(-\mathbf{k}) = \Theta V(\mathbf{k})\Theta^{-1}. \qquad (4)$$

It is straightforward to enumerate the allowed terms for each SG. In general, there are 28 terms consistent with inversion and T. Eqs. 2-4 determine the $\mathbf{k}$ dependence of each term. Here, in order to faithfully characterize the degeneracy pattern of the band structures we consider a simplified model with a subset of crystal field, hopping and spin orbit terms that respect (4) and are sufficient to lift all nonessential degeneracies. These qualitative features are reflected in the specific materials band structures discussed in the supplementary materials.

$$V_{130} = \lambda_1\tau^z\mu^y\cos\tfrac{k_z}{2} + \lambda_2\tau^z(\sigma^x\sin k_y - \sigma^y\sin k_x) + \lambda_3\tau^x\mu^z(\sigma^x\sin\tfrac{k_x}{2}\cos\tfrac{k_y}{2} + \sigma^y\cos\tfrac{k_x}{2}\sin\tfrac{k_y}{2}), \quad (5)$$

and

$$V_{135} = t_1'\mu_z(\cos k_x - \cos k_y) + t_2'\tau^y\mu^y \sin\tfrac{k_x}{2}\sin\tfrac{k_y}{2}\cos\tfrac{k_z}{2}$$
$$+\ \lambda_1'\tau^y\mu^x(\sigma^x \sin\tfrac{k_x}{2}\cos\tfrac{k_y}{2} + \sigma^y\cos\tfrac{k_x}{2}\cos\tfrac{k_y}{2})\sin\tfrac{k_z}{2}$$
$$+\ \lambda_2'\tau^x\mu^y(\sigma^x \cos\tfrac{k_x}{2}\sin\tfrac{k_y}{2} + \sigma^y\sin\tfrac{k_x}{2}\cos\tfrac{k_y}{2})\sin\tfrac{k_z}{2}$$
$$+\ \lambda_3'\tau^y\mu^z\sigma^z\cos\tfrac{k_x}{2}\cos\tfrac{k_y}{2}(\cos k_x - \cos k_y). \quad (6)$$

Fig. 1(c,d) show energy bands associated with these models. Each band is at least doubly degenerate. Both cases feature a DDP at A with linear dispersion in all directions. SG 130 features an additional fourfold crossing along the line Z-R. This crossing is protected by T, inversion and the C_{2x} screw, whose axis is displaced from the center of inversion. This guarantees that the Kramers-degenerate pairs of states on this line share the same eigenvalue of the C_{2x} screw, allowing pairs with different eigenvalues to cross. A similar crossing occurred in the Dirac ring found in Refs. 11 and 14 and was locally characterized in Ref. 27. In fact, this crossing is *guaranteed* by symmetry, since it is not possible to eliminate it by reordering the bands at Z or at R. This pattern of degeneracies guarantees that groups of 8 bands stick together, independent of the DDP at A, and appears to be correlated with the WPVZ bound.

Since the additional Dirac points need not be at the same energy as the DDP, SG 130 will generically be a semimetal with electron and hole pockets. In contrast, SG 135 has no additional Dirac points, so it can host an intrinsic DDSM. However, we find that for $\lambda_2' > \lambda_1'$ there are additional single Dirac points along the lines A-Z. These arise due to a "velocity inversion" transition at $\lambda_2' = \lambda_1'$, which we analyze below. A similar velocity inversion occurs in 130 for $\lambda_3 > 2\lambda_2$.

We now focus on SG 135 and consider the low energy structure near the DDP. There are no symmetry-respecting terms at A that lift the degeneracy. To determine the terms linear in $\mathbf{k}$ we identify the T-odd operators transforming in the vector representations of the point group D_{4h}. Using (2-4), the representations of the symmetry operations at A are $d_A(\{C_{4z}|00\frac{1}{2}\}) = \tau^z\mu^x \exp i\pi\sigma^z/4$, $d_A(\{C_{2x}|\frac{1}{2}\frac{1}{2}0\}) = \tau^y\mu^z\sigma^x$ and $d_A(\{I|000\}) = \mu^z$. Also, $\Theta_A = i\mu^z\sigma^y K$. We find 4 (3) terms with E_u (A_{2u}) symmetry, in agreement with the general analysis of Table I. The $\mathbf{k}\cdot\mathbf{p}$ Hamiltonian at A is

$$\mathcal{H}_{\mathcal{A}} = (u_0\tau^x\mu^y\sigma^x + u_1\tau^y\mu^x\sigma^y + u_2\mu^y\sigma^y + u_3\tau^z\mu^y\sigma^x)k_x$$
$$+\ (u_0\tau^x\mu^y\sigma^y + u_1\tau^y\mu^x\sigma^x + u_2\mu^y\sigma^x - u_3\tau^z\mu^y\sigma^y)k_y$$
$$+ (v_1\mu^x + v_2\tau^y\mu^y + v_3\tau^x\mu^y\sigma^z)k_z. \quad (7)$$

This leads to dispersion

$$E^2_\pm(\mathbf{k}) = (|\mathbf{u}|^2 + u_0^2)(k_x^2+k_y^2) + |\mathbf{v}|^2k_z^2$$
$$\pm 2\sqrt{4k_x^2k_y^2|\mathbf{u}|^2u_0^2 + (k_x^2+k_y^2)k_z^2(\mathbf{u}\cdot\mathbf{v})^2}, \quad (8)$$

A_{1g}	1	Double Dirac SM
A_{2g}	$\tau^x\mu^z \quad \tau^y\mu^z\sigma^z \quad \tau^z$	Weak TI
B_{1g}	μ^z	Strong TI
B_{2g}	$\tau^x \quad \tau^y\sigma^z \quad \tau^z\mu^z$	Weak TI
$E_g^{x,y}$	$\tau^y\sigma^{x,-y} \quad \tau^y\mu^z\sigma^{x,y}$	Dirac Line/Point SM
A_{1u}	$\tau^x\mu^y \quad \tau^y\mu^y\sigma^z \quad \mu^x\sigma^z$	Strong TI
A_{2u}	$\tau^z\mu^z\sigma^z$	Dirac Point SM
B_{1u}	$\tau^z\mu^y$	Weyl Point SM
B_{2u}	$\tau^x\mu^x\sigma^z \quad \tau^y\mu^x \quad \mu^y$	Weyl Point SM
$E_u^{x,y}$	$\tau^x\mu^x\sigma^{x,-y} \quad \tau^z\mu^x\sigma^{x,y}$ $\tau^y\mu^y\sigma^{y,-x} \quad \mu^x\sigma^{y,-x}$	Weyl Point SM

TABLE III. Perturbations to the DDP in SG 135, classified by their symmetry under the D_{4h} point group[23]. The resulting insulating and semimetallic (SM) phases are indicated.

where $\mathbf{u} = (u_1, u_2, u_3)$ and $\mathbf{v} = (v_1, v_2, v_3)$. When $|u_0| = |\mathbf{u}|$, one of the branches vanishes on the line $k_x = k_y$, $k_z = 0$, identifying the velocity inversion transition along A-Z discussed above. From the tight-binding model, we have $\mathbf{u} = (\lambda_1', 0, 0)$, $u_0 = \lambda_2'$, so we identify $|u_0| < |\mathbf{u}|$ with the intrinsic DDSM phase with no additional degeneracies.

Lowering the symmetry by external perturbations, such as strain, provides a powerful tool for engineering gapped topological phases[28, 29] We therefore consider the long-wavelength symmetry-breaking perturbations that open energy gaps and identify the resulting phases that arise. General symmetry-breaking perturbations are classified by their symmetries under the D_{4h} point group, which can be determined from $d_A(\{g|\mathbf{t}\})$, as above. The possible T-invariant perturbations at A are listed in Table III. There are many terms, and their effects depend on the form of the velocity terms. In order to organize the behavior, we first fix the velocity terms and examine the terms that can open a gap in the spectrum. We find that there are precisely four mass terms that arise due to perturbations with specific symmetries. The Hamiltonian has the form

$$\mathcal{H} = u_2\mu^y(\sigma^yk_x + \sigma^xk_y) + v_1\mu^xk_z + m_{A_{2g}}\tau^x\mu^z +$$
$$m_{B_{2g}}\tau^z\mu^z + m_{B_{1g}}\mu^z + m_{A_{1u}}\tau^y\mu^y\sigma^z. \quad (9)$$

The four mass terms are the unique terms from Table III that anticommute with all three of the velocity terms and open a gap. They fall into two groups. $\mathbf{m}_1 = (m_{A_{2g}}, m_{B_{2g}})$ and $\mathbf{m_2} = (m_{B_{1g}}, m_{A_{1u}})$ anticommute among themselves but commute with each other, leading to an energy gap $E_{\rm gap} = 2|m|$ with $m = |\mathbf{m}_1| - |\mathbf{m}_2|$. There are two phases distinguished by $\mathrm{sgn}(m) = +1(-1)$. Using parity eigenvalues [28, 30], we identify them as a $[0; 110]$ weak TI ($[1; 001]$ strong TI). While these indices depend on the details of the band structure away from the DDP, the difference between the phases is robust. To visualize the phases, Fig. 2(a) shows a phase diagram for $m_{A_{1u}} = 0$. In this 3D space, the STI (WTI) are inside (outside) a cone. In the more general 4D phase diagram, the WTI and STI phases appear symmetrically.

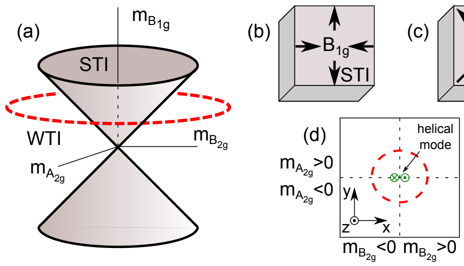

FIG. 2. (a) Phase diagram as a function of 3 symmetry-breaking perturbations. A topologically nontrivial loop in the WTI phase is indicated by the dashed circle. (b,c) Uniaxial strain along different directions leads to topologically distinct insulating states. (d) A topological line defect in an insulating state binds a gapless 1D helical mode.

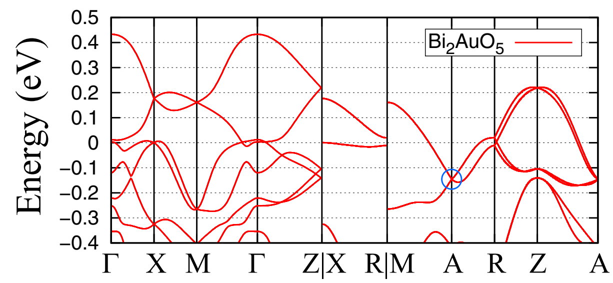

FIG. 3. (a) Band structure of Bi_2AuO_5 in SG 130, obtained from first-principles calculations. The DDP appears at A with extra Dirac points along R-Z. See the supplementary material for the methods.

Different combinations of velocity terms lead to different choices for the anticommuting mass terms. However, for any combination of velocity terms in (7), it can be exhaustively checked that there is one anticommuting term with each of the symmetries in Eq. 9. Therefore, a generic perturbation with a given symmetry induces the corresponding mass term and opens a gap. The general structure of Fig. 2(a) remains, except that when the inversion-symmetry-breaking term $m_{A_{1u}}$ is present the boundary between the STI and WTI phases broadens to include a Weyl semimetal phase [31].

The dependence of the topological state on $m_{B_{1g}}$ and $m_{B_{2g}}$ provides a mechanism for controlling topological states using strain. As indicated in Fig.2(b,c), uniaxial strain along the x or y directions induces a perturbation with a combination of A_{1g} and B_{1g} symmetry, while uniaxial strain along the diagonal $x \pm y$ directions has A_{1g} and B_{2g} symmetry. Therefore these two kinds of compressive strain lead to topologically distinct insulators.

DDPs can also be differentiated from single Dirac semimetals by the existence of two distinct anticommuting mass terms that lead to the same topological phase. For a single Dirac semimetal with 4×4 Dirac matrices, the general structure of Clifford algebras predicts that there is only a single T-invariant mass term that anticommutes with the three T-odd anticommuting velocity terms. For 8×8 Dirac matrices there are *two* anticommuting T-invariant mass terms. This means that the space of gapped states has a nontrivial first homotopy group, indicated by the dashed circle in Fig. 2(a), allowing topologically nontrivial *line defects* (Fig. 2(d)). Line defects in a 3D insulator in class AII have a Z_2 topological invariant characterizing the $3+1$D $\mathcal{H}(\mathbf{k}, \theta)$ [32]. When nontrivial, this guarantees that a 1D helical mode is bound to the line, similar to the helical mode bound to a lattice dislocation in a weak TI [33]. Without a lattice dislocation, this Z_2 invariant is inaccessible in a 4 band system because it derives via dimensional reduction [34] from a *third* Chern number in $3+1+2$D, which requires at least 8 bands. To establish that a line defect binds a 1D helical mode, we follow the analysis of Ref. 32, and consider a simple model with $m_{B_{2g}} = ax$, $m_{A_{2g}} = ay$ and $u_1 = v_2 = v$. $\mathcal{H}^2$ in (9) then has the form of a harmonic oscillator, and there is a single pair of modes with $E = \pm v k_z$ localized near $x = y = 0$.

We finally briefly consider perturbations in Table III with the remaining symmetries, which lead to Weyl or Dirac semimetals. The E_g perturbations lead to either Dirac points or a Dirac ring, with fourfold-degenerate crossings. The inversion breaking-perturbations generally lead to a Weyl semimetal with twofold crossings, except for A_{2u}, where the remaining C_{2z} and glide mirror symmetries guarantee doubly-degenerate states for $k_x = k_y = \pi$ with the same C_{2z} eigenvalue. This allows degenerate bands to cross along A-M, protecting a Dirac point even though inversion is violated.

Encouragingly, the DDP appears to be feasible in known materials [35]. For example, a ternary bismuth aurate, Bi_2AuO_5 in SG 130, which has been synthesized in a single crystal [36], hosts a DDP at A close to the Fermi level, with additional four-fold degeneracies appearing on Z-R (Fig. 3). As for materials in SG 135, the MATERIALS PROJECT [37] shows that a class of oxide materials isostructural with Pb_3O_4 [38], including $Sn(PbO_2)_2$, Pb_3O_4, and $Mg(PbO_2)_2$, host the DDPs in the valence energy regime. Although they are semiconductors with electron filling 8, their atomic structure allows for a potential route towards a material design that shifts the Dirac point near the Fermi level. The number of atoms per each species in a unit cell is 4 (mod 8) and thus allows for filling 4 when suitably substituting atoms with an odd number of valence electrons. In SG 223, $GaMo_3$ [39] hosts a DDP. There is reason for optimism that with appropriate band structure engineering, an intrinsic DDSM can be realized.

We thank Eugene Mele and Steve Young for helpful discussions. This work was supported by NSF grant DMR 1120901 and a Simons Investigator grant to CLK from the Simons Foundation. AMR acknowledges the support of the DOE, under grant DE-FG02-07ER46431.

[1] A. H. C. Neto, N. M. R. Peres, K. S. Novoselov, and A. K. Geim, Rev. Mod. Phys. **81**, 109 (2009).
[2] M. Z. Hasan and C. L. Kane, Rev. Mod. Phys. **82**, 3045(2010); X.-L. Qi and S.-C. Zhang, Rev. Mod. Phys. **83**, 1057 (2011).
[3] X. Wan, A. M. Turner, A. Vishwanath, and S. Y. Savrasov, Phys. Rev. B **83**, 205101 (2011).
[4] S. M. Young, S. Zaheer, J. C. Y. Teo, C. L. Kane, E. J. Mele, and A. M. Rappe, Phys. Rev. Lett. **108**, 140405 (2012).
[5] Z. Wang, Y. Sun, X.-Q. Chen, C. Franchini, G. Xu, H. Weng, X. Dai, and Z. Fang, Phys. Rev. B **85**, 195320 (2012).
[6] Z. Wang, H. Weng, Q. Wu, X. Dai, and Z. Fang, Phys. Rev. B **88**, 125427 (2013).
[7] Z. K. Liu, B. Zhou, Y. Zhang, Z. J. Wang, H. M. Weng, D. Prabhakaran, S.-K. Mo, Z. X. Shen, Z. Fang, X. Dai, Z. Hussain, and Y. L. Chen, Science **343**, 864867 (2014).
[8] Z. K. Liu, J. Jiang, B. Zhou, Z. J.Wang, Y. Zhang, H. M. Weng, D. Prabhakaran, S.-K. Mo, H. Peng, P. Dudin, T. Kim, M. Hoesch, Z. Fang, X. Dai, Z. X. Shen, D. L. Feng, Z. Hussain, and Y. L. Chen, Nat. Mater. **13**, 677681 (2014).
[9] S. Borisenko, Q. Gibson, D. Evtushinsky, V. Zabolotnyy, B. Büchner, and R. J. Cava, Phys. Rev. Lett. **113**, 027603 (2014).
[10] J. A. Steinberg, S. M. Young, S. Zaheer, C. L. Kane, E. J. Mele, and A. M. Rappe, Phys. Rev. Lett. **112**, 036403 (2014).
[11] J. M. Carter, V. V. Shankar, M. A. Zeb, and H.-Y. Kee, Phys. Rev. B **85**, 115105 (2012).
[12] H. Weng, Y. Liang, Q. Xu, R. Yu, Z. Fang, X. Dai, and Y. Kawazoe, Phys. Rev. B **92**, 045108 (2015).
[13] G. E. Volovik, J. Supercond. Nov. Magn. **26**, 2887 (2013).
[14] H.-S. Kim, Y. Chen, and H.-Y. Kee, Phys. Rev. B **91**, 235103 (2015).
[15] Y. Chen, Y.-M. Lu, and H.-Y. Kee, Nat. Commun. **6**, 6593 (2015).
[16] H. Weng, C. Fang, Z. Fang, B. A. Bernevig, and X. Dai, Phys. Rev. X **5**, 011029 (2015).
[17] Y. Kim, B. J. Wieder, C. L. Kane, A. M. Rappe, Phys. Rev. Lett. **115**, 036806 (2015).
[18] R. Yu, H. Weng, Z. Fang, X. Dai, and X. Hu, Phys. Rev. Lett. **115**, 036807 (2015).
[19] L. S. Xie, L. M. Schoop, E. M. Seibel, Q. D. Gibson, W. Xie, and R. J. Cava, (2015), APL Mat. **3**, 083602 (2015).
[20] Z. Wang, D. Gresch, A. A. Soluyanov, W. Xie, S. Kushwaha, X. Dai, M. Troyer, R. J. Cava and B. A. Bernevig, arXiv:1511.07440 (2015).
[21] S. M. Young and C. L. Kane, Phys. Rev. Lett. **115**, 126803 (2015).
[22] L. M. Schoop, M. N. Ali, C. Strasser, V. Duppel, S.S. P. Parkin, B. V. Lotsch and C. R. Ast, arXiv:1509.00861 (2015).
[23] C. J. Bradley and A. P. Cracknell, "The Mathematical Theory of Symmetry in Solids" (Clarendon Press Oxford, 1972).
[24] A similar analysis for single groups without spin-orbit interactions was carried out in J. L. Mañes, Phys. Rev. B **85**, 155118 (2012).
[25] H. Watanabe, H. C. Po, A. Vishwanath, M. P. Zaletel, Proc. Natl. Acad. Sci. **112**, 14551 (2015).
[26] S. Groves and W. Paul, Phys. Rev. Lett. **11**, 194 (1963).
[27] C. Fang, Y. Chen, H.-Y. Kee, L. Fu, Phys. Rev. B **92**, 081201 (2015).
[28] L. Fu and C.L. Kane, Phys. Rev. B **76**, 045302 (2007).
[29] C. Brüne, C.X. Liu, E. G. Novik, E. M. Hankiewicz, H. Buhmann, Y. L. Chen, X. L. Qi, Z. X. Shen, S. C. Zhang, and L. W. Molenkamp, Phys. Rev. Lett. **106**, 126803 (2011).
[30] L. Fu, C.L. Kane and E.J. Mele, Phys. Rev. Lett. **98**, 106803 (2007).
[31] S. Murakami, New Journ. of Phys. **9**, 356 (2007).
[32] J.C.Y. Teo and C.L. Kane, Phys. Rev. B **82**, 115120 (2010).
[33] Y. Ran, Y. Zhang, and A. Vishwanath, Nat. Phys. **5**, 298 (2009).
[34] X.-L. Qi, T. L. Hughes, and S.-C. Zhang, Phys. Rev. B **78**, 195424 (2008).
[35] See Supplemental Material [url], which includes Refs. [40–44], for the band structures.
[36] J. Geb and M. Jansen, J. Solid State Chem. **122**, 364 (1996).
[37] A. Jain, S. P. Ong, G. Hautier, W. Chen, W. K. Richards, S. Dacek, S. Cholia, D. Gunter, D. Skinner, G. Ceder and K.A. Persson, APL Materials **1**, 011002 (2013).
[38] J. R. Gavarri, J. P. Vigouroux, G. Calvarin and A. W. Hewat, J. Solid State Chem. **36**, 81 (1981).
[39] J. Bornand, R. Siemens, and L. Oden, Journal of the Less Common Metals **30**, 205 (1973).
[40] J.P. Perdew, K. Burke, and M. Ernzerhof, Phys. Rev. Lett. **77**, 3865 (1996).
[41] P. Giannozzi *et al.*, J. Phys. Condens. Mat. **21**, 395502 (2009).
[42] A. M. Rappe, K. M. Rabe, E. Kaxiras, and J. D. Joannopoulos, Phys. Rev. B **41**, 1227 (1990).
[43] N. J. Ramer and A. M. Rappe, Phys. Rev. B **59**, 12471 (1999).
[44] Inorganic Crystal Structure Database (ICSD), (Fachinformationszentrum Karlsruhe, Karlsruhe, Germany, 2015).